# Transition Metal Dichalcogenides/Gold-Based Surface Plasmon Resonance Sensors: Exploring the Geometrical and Material Parameters

Pericle Varasteanu[1,2]

## Abstract

In this study, we explored the geometrical and material parameters of surface plasmon resonance (SPR) sensors, in order to gain insight about the mechanisms that control the sensors' response when different 2D materials monolayers ($MoS_2$, $MoSe_2$, $WS_2$, $WSe_2$) are used to modify the surface. Accordingly, the surface plasmons' (SPs) dispersion relations, the reflectivity maps and both reflectivity and phase responses for the visible and near-infrared wavelengths range (400–1400 nm), were systematically investigated by using COMSOL Multiphysics (RF Module) and transfer matrix method (TMM) algorithm considering a modified Kretschmann configuration. We showed that the sensitivity of the modified structures is enhanced for wavelengths between 600 and 1000 nm both in reflectivity and phase. By evaluating also the influence of the number of 2D material monolayers, the highest sensitivity in reflectivity was obtained at 700 nm when five monolayers of $MoS_2$ were added, reaching 220 deg/RIU for a change in dielectric's refractive index of 0.002 RIU, which is 45% higher than that of the standard bare structure. Regarding the phase response, it was shown that by adding only one monolayer of $MoS_2$, a sensitivity of $9 \times 10^5$ deg/RIU is achieved for a refractive index change of $10^{-6}$ RIU.

**Keywords** SPR sensor · 2D materials · Dispersion relations · Sensitivity enhancement · Phase response

## Introduction

The interaction between electromagnetic radiation and mobile surface charges, generally the electrons from the conduction band in metals, highly doped semiconductors [1], or conducting polymers [2], gives rise to a special type of surface wave called surface plasmons (SPs) due to the induced collective oscillations of electrons [3]. The SPs are bounded electromagnetic modes having a greater wave vector than the incidence light at the same wavelength which lead to an exponentially (evanescent) decay of their electromagnetic field intensity with the distance away from the surface, being highly sensitive to the surrounding dielectric constant. The mismatch between the SPs' wave vector and the one of the incidence light forbids the coupling, but under special configurations the light wave vector could be increased until it matches the one of the SP's leading thus to a resonant energy transfer between the incident light and the SP's. In Kretschmann configuration, an optical prism is used to increase the light's wave vector only by modifying the incidence angle. The resonance can be seen as a sharp drop of the reflected wave intensity, and the angle at which the intensity is close to 0 is called the resonance angle $\theta_{res}$. Mathematically, the resonance condition can be expressed as $k_0 \sqrt{\frac{\varepsilon_m \varepsilon_d}{\varepsilon_m + \varepsilon_d}} = k_0 n_p \sin\theta$, where the left side of the equation represents the SPs wave vector and the right side is the incidence light wave vector with propagating through prism. $k_0$ is free space wave vector, $\varepsilon_m$, $\varepsilon_d$ represent the dielectric constant of metal and dielectric, respectively, $n_p$ is the prism refractive index, and $\theta$ is the angle of incidence. The SP's wavevector varies with the changes in the surrounding medium's dielectric constant (refractive index), and, consequently, in order to fulfill the resonance condition, the incidence angle should be also modified. The displacement of the resonance angle at a variation of the surrounding medium's refractive index measures the sensor sensitivity.

✉ Pericle Varasteanu
  pericle.varasteanu@imt.ro

1   National Institute for Research and Development in Microtechnology (IMT Bucharest), 126A Erou Iancu Nicolae Street, 077190 Voluntari, Romania

2   Faculty of Physics, University of Bucharest, 405 Atomistilor Street, RO-077125 Magurele, Romania

Since the first configurations proposed to excite the surface plasmons by Otto, Kretschmann, and Raether [4, 5], these techniques showed a great potential for studies that requires high sensitivity and high specificity. Among them, studies focused on temperature variations in the vicinity of metal surface or even metal temperature [6], surface roughness [5] and recently, measurements of the metal dielectric constant [7] were reported. Nowadays, due to their high sensitivity, the surface plasmon resonance (SPR) sensors are mainly used to quantify the biomedical interactions, where the sample volumes and concentrations are very small, and the labeling processes could induce structural modifications of the molecules. Thus, their use was reported for detection of the mutations in circulating cell free DNA [8, 9], study of protein-DNA interactions [10], or identification of human blood group [11]. Furthermore, the real time detection of the induced surface reactions and the relatively simple and inexpensive setup was another reason for choosing the SPR-based detection [12]. The sensitivity of gold film SPR (bio)sensors is known to be limited for small molecules (< 500 Da) [13]. In order to overcome this limitation, various sensor configurations were studied: (i) silver was used for the metallic layer instead of gold exhibiting better performances than the gold sensors regarding the full width at half maximum (FWHM) of the reflectivity curve, but the feeble chemical stability of silver hinders its further development [14]; (ii) bimetallic silver-gold platforms, where the narrower resonance curve response attributed to silver and the higher resonance angle displacement of gold were combined resulting thus in a high sensitivity and a low signal to noise ratio sensor [15]. In addition to these bare metal configurations, it was reported that the sensor's response could be improved by coating the metal with thin dielectric films [16–19]. The remarkable optoelectronic properties attributed to the unique band structure [20] and enhanced biocompatibility due the absorption of molecules by the $\pi$-$\pi$ stacking [21] of graphene have drawn a lot of attention resulting thus in a new type of highly sensitive SPR sensor's configurations: (i) metal-graphene monolayers [22], (ii) metal-thin dielectric film-graphene monolayers [23], and (iii) bimetallic structure (Ag-Au)-graphene monolayers [24]. The main drawback of the sensors coated with graphene is that the sensitivity starts to improve only when more than 5–6 monolayers were added and also the additional damping due to the larger imaginary part for a higher number of monolayers decrease sensitivity [25, 26]. As a solution for these shortcomings, the transition metal dichalcogenide (TMDC) materials, considered the emerging 2D monolayers due to their excellent optoelectronic and biocompatibility properties [26], were explored with promising results as possible candidates to further improve the sensitivity by coating the graphene-based sensors [27, 28] or even to replace the graphene monolayers. In this context, it was demonstrated that TMDC exhibit greater absorption of light than graphene monolayers, achieving thus

higher sensitivities with a smaller number of monolayers stacked [29]. Among them, $MoS_2$- and $WS_2$-based SPR configurations were extensively studied in literature [30–32].

However, despite the increased number of studies focused on utilization of 2D materials to increase the sensing performances of SPR sensors, a systematical comparison of the influence of disulfides and diselenides in terms of both reflectivity and phase response is still lacking. Thus, the primary goal of this study is to gain an insight about the properties of gold (Au) surfaces coated with 2D TMDC materials monolayers for SPR (bio)sensing applications by exploring the geometrical and material space parameters of the sensors and studying the relation dispersions, reflectivity maps and sensitivities in reflectivity and phase, respectively, for wavelengths in the VIS (400–700 nm) and NIR (700–1400 nm) part of the electromagnetic spectrum. The study was conducted on 4 sensors new configurations (Au-$MoS_2$, Au-$MoSe_2$, Au-$WS_2$, and Au-$WSe_2$, respectively) varying the number of layers in comparison with the classic bare gold structure. Furthermore, in order to diminish the differences between theoretical results and the experimental ones in the proposed geometry, we took into account the presence of the chromium adhesion layer [33].

## Theoretical Analysis of Sensor's Performance Parameters

The Kretschmann configuration as the most widely used SPR-based sensor structure was employed to explore the impact of using additional $MX_2$ 2D monolayers on the performance parameters, including their effect on the sensitivity and SPP coupling (Fig. 1). In this configuration, the coupling prism
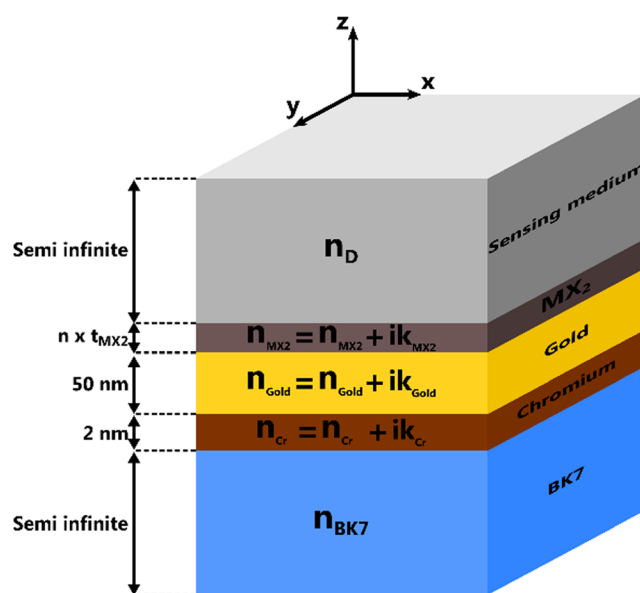


**Fig. 1** Schematic diagram of the $MX_2$ modified SPR sensor

material is borosilicate-crown glass (BK7) and the metallic layer with plasmonic properties in visible and near-infrared region is gold (Au).

Firstly, the optical characteristics of the $MX_2$ modified SPR sensors were analyzed numerically in the entire visible and near-infrared regions of the light spectrum (400–1400 nm), using the transfer matrix method (TMM) that becomes a requisite in simulating the optical properties, such as reflectivity, absorption, and transmission and it is based on computing the Fresnel equations for multiple layers [34]. The optical parameters that define each of the layers, such as refractive indices for different wavelengths [35, 36], are shown in Table 1. Regarding the geometrical parameters used for the different layers employed in our optical platform design, they were chosen taking into account the most commonly used values in literature for the classic Kretschmann configuration [29, 36]. Furthermore, for the consistency of our numerical results, we took into account the presence of the chromium adhesion layer, considering the thickness generally used in our experimental studies.

Two assumptions were made regarding the $MX_2$ layers: (i) the interfaces phenomena between the $MX_2$ monolayers were neglected, and (ii) the presence of multiple $MX_2$ layers was reflected only as increased thickness, defined as: $m \times t_{MX_2}$, where $m$ represents the number of layers and $t_{MX_2}$ is the thickness of one monolayer, whereas the complex refractive index remains the same as for one monolayer.

For the sake of completeness, we present below TMM algorithm [34]. The algorithm starts by considering the tangential fields at the first boundary to be linked to those at the final boundary by the following matrix relation:

$$\begin{bmatrix} U_1 \\ V_1 \end{bmatrix} = M \begin{bmatrix} U_{N-1} \\ V_{N-1} \end{bmatrix}, \tag{1}$$

where $M$ represents the characteristic matrix of the system which was given by:

$$M = \prod_{k=2}^{N-1} M_k = \begin{bmatrix} M_{11} & M_{12} \\ M_{21} & M_{22} \end{bmatrix} \tag{2}$$

$$M_k = \begin{bmatrix} \cos\beta_k & \dfrac{-i\sin\beta_k}{q_k} \\ -iq_k\sin\beta_k & \cos\beta_k \end{bmatrix} \tag{3}$$

$$\beta_k = \frac{2\pi d_k \left( \sqrt{\epsilon_k - n_1^2 \sin^2\theta_1} \right)}{\lambda}, \tag{4}$$

where $d_k$ represents the thickness of layer $k$, $\epsilon_k$ is the dielectric constant of layer $k$, $n_1$ is the refractive index of coupling prism, $\theta_1$ is the angle of incidence, and $\lambda$ is the incidence wavelength of light.

The variable $q_k$ is different for the two polarizations, TM (p-polarized) and TE (s-polarized). Accordingly, for TM it is given by equation:

$$q_k^p = \frac{\sqrt{\epsilon_k - n_1^2 \sin^2\theta_1}}{\epsilon_k} \tag{5}$$

For TE polarization, it is:

$$q_k^s = \sqrt{\epsilon_k - n_1^2 \sin^2\theta_1} \tag{6}$$

Reflection coefficient for the two polarizations can be calculated by plugging in the appropriate expression for $q_k$ in $M_k$:

$$r_{p,s} = \frac{q_1^{p,s}\left(M_{11} + q_N^{p,s} M_{12}\right) - \left(M_{21} + q_N^{p,s} M_{22}\right)}{q_1^{p,s}\left(M_{11} + q_N^{p,s} M_{12}\right) + \left(M_{21} + q_N^{p,s} M_{22}\right)} \tag{7}$$

Thus, following the calculations, the reflectivity was obtained by taking the square of reflection coefficient's absolute value and real part of reflection coefficient and can be calculated by taking the argument

$$R_p = |r_p|^2 \tag{8}$$

Phase represents the relation between the imaginary of reflection coefficient:

$$\Phi = \mathrm{atan}\left(\frac{\mathrm{Im}(r_p)}{\mathrm{Re}(r_p)}\right) = \arg(r_p) \tag{9}$$

In this paper we considered the sensitivity in angular interrogation for reflectivity response as the displacement of the resonance angle with the change in refractive index of the sensing medium, and the corresponding formula used to calculate the reflectivity sensitivity is:

$$S_r = \frac{\Delta\theta_{res}}{\Delta n} \tag{10}$$

where $\Delta\theta_{res}$ is the displacement of the resonance angle and $\Delta n$ is the change in sensing medium's refractive index which was set to 0.002 relative refractive index units (RIU). For the reflectivity response, only TM (p-polarization) was considered, because, in such configuration, the surface plasmons cannot be excited by TE (s-polarization) of the light.

The sensitivity of the phase response is similar to the one corresponding to reflectivity, but, in this case, instead of the resonance angle variation, we have considered the differential phase variation as function of the change in sensitive medium's refractive medium. Since the light in TE polarization cannot excite the SPR, it is used as a reference signal for improving the sensing resolution and for removing the

**Table 1** Complex refractive indices ($n = n + ik$) of materials used in TMM algorithm (three wavelengths were chosen as 700, 900, 1300 nm, respectively) [35, 36]

| Material | Thickness [nm] | Wavelength [nm] | | |
|---|---|---|---|---|
| | | 700 | 900 | 1300 |
| BK7 | – | $n = 1.5131$ | $n = 1.5090$ | $n = 1.5037$ |
| Cr | 2 | $n = 3.0536$ | $n = 3.3096$ | $n = 3.6795$ |
| | | $k = 3.3856$ | $k = 3.5243$ | $k = 3.7139$ |
| Au | 50 | $n = 0.1310$ | $n = 0.1744$ | $n = 0.3880$ |
| | | $k = 4.0624$ | $k = 5.7227$ | $k = 8.7970$ |
| MoS$_2$ | 0.65 | $n = 5.8429$ | $n = 4.7331$ | $n = 4.3350$ |
| | | $k = 0.2509$ | $k = 0.1200$ | $k = 0.0570$ |
| MoSe$_2$ | 0.7 | $n = 4.1150$ | $n = 3.9890$ | $n = 3.6640$ |
| | | $k = 1.0570$ | $k = 0.4430$ | $k = 0.2610$ |
| WS$_2$ | 0.8 | $n = 5.4270$ | $n = 5.1303$ | $n = 4.7150$ |
| | | $k = 0.3604$ | $k = 0.2511$ | $k = 0.1550$ |
| WSe$_2$ | 0.7 | $n = 5.1730$ | $n = 4.9720$ | $n = 4.4420$ |
| | | $k = 0.4010$ | $k = 0.2480$ | $k = 0.1550$ |

external noise [18, 24]. The following formula was used for calculations:

$$S_\phi = \frac{\Delta \phi_d}{\Delta n} \tag{11}$$

where $\phi_d$ is the differential phase defined as $|\phi_P - \phi_S|$ and $\phi_{p,s}$ represents the phase response for TM and TE polarization, respectively.

## Results and Discussion

Our study is focused firstly on the evaluation of two optical quantities relevant for any new sensor chip or optical platform design, such as electric field confinement and penetration depth that determine the functional parameters in order to make the surface plasmon mode to strongly depend to the changes in sensitive medium refractive index. This quantities might determine the sensitivity (i.e., a higher effective index means a shorter penetration depth in media, fact which leads to a high field confinement at the interface between metal and dielectric, and a decrease in the phase velocity) [5]. In order to evaluate the aforementioned quantities, we started by calculating the dispersion relations for the investigated structures for different MX$_2$ materials. The dispersion relations were numerically calculated using COMSOL Multiphysics software, which computes the effective index or propagation constant of a 2D waveguide geometry. For this step, we employed a bare structure consisting of a dielectric with a fixed refractive index $n = 1.33$ placed on the top of a gold substrate. For the modified structures, we considered the additional MX$_2$ layers

placed between the gold substrate and the sensing layer. The thicknesses and refractive indices of the MX$_2$ layers are shown in Table 1.

It can be seen that at shorter wavelengths the modified structures exhibit higher effective indices than that of the bare structure, while at longer wavelengths the values of the effective indices for all structures become approximately equal implying that at these wavelengths the sensor's performances are the same as the ones for the bare structure. Different values for the effective indices for the modified structures arise due to the optical properties of the MX$_2$ layers. An important parameter that shows the length scale in which the surface plasmons are sensitive for differences in refractive indices of the sensing medium is the penetration depth which can be obtained directly from the dispersion relations using the simple relation:

$$\delta_{m,(d)} = \frac{1}{\left| k_0 \sqrt{n_{eff}^2 - \epsilon_{m(d)}} \right|} \tag{12}$$

where $k_0$ represents the free space wave vector, and $\epsilon_{m(d)}$ is the dielectric constant of the metal and for the dielectric layer depending which layer is studied.

The inset of Fig. 2 shows the z component of the electric field for the bare structure (dashed lines) and for the modified structures (solid line) at three different wavelengths. For longer wavelengths, the field intensity in the proximity of the gold layer is reduced and penetration depth is increased. The increase in penetration depth is due to the property of the gold layer to be a better conductor at longer wavelengths which leads consequently to a less confined mode at the interface [37] The shorter penetration depth of the modified structures caused by the higher effective index indicates that the field confinement at the dielectric–metal interface is enhanced in comparison to the case of the bare structure. This fact makes the modified structures more sensitive to smaller molecules
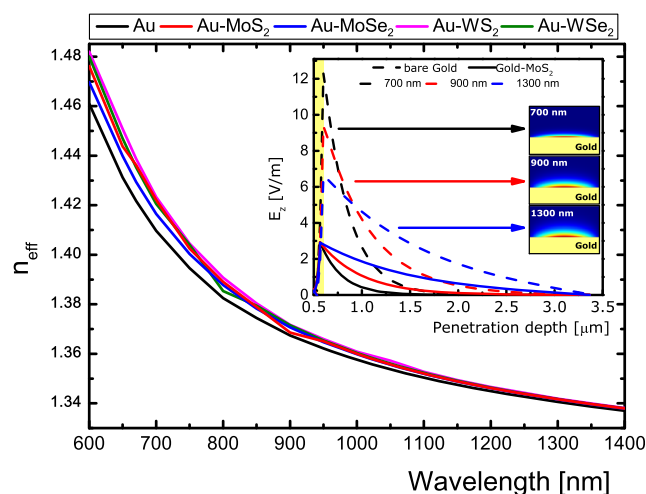


**Fig. 2** Dispersion relations for all of the proposed sensor configurations for a sensing medium refractive index of 1.33

near the interface. Another feature that can be observed from the electric field profile is that the penetration depth for the modified structures increases with the wavelength while the maximum field amplitude remains the same for the three wavelengths. At longer wavelengths, the surface plasmons are no longer sensitive to the changes in the dielectric medium, the effective indices for the modified structures being approximately equal with the one of bare Au structure.

In order to gain more insight about the sensor's behavior for different numbers of $MX_2$ layers added on top of the metal, we calculated the reflectivity maps representing the dependence of the reflectivity as a function of the wavelength and the angle of incidence using the transfer matrix method presented in "Theoretical Analysis of Sensor's Performance Parameters" section. Thus, the reflectivity maps complete the information obtained from standard dispersion relations [19]. The results obtained for both bare Au structure and the modified structures with layers of 2D materials: $MoS_2$, $MoSe_2$, $WS_2$, and $WSe_2$, when the incident radiation wavelengths range from 0.4 to 1.4 μm and for incidence angles between 60 and 89°, are presented in Fig. 3. The wavelength step used was 0.01 μm and angular step was 0.003 deg.

The loss character of the metal, quantified by the complex dielectric constant, imposes limitations on the SP' wave vector as well as on the field confinement at the interface. In contrast to the case of lossless metal, where the wavevector tends to infinity at resonant SP frequency, for the lossy case the SP wavevector acquires a finite value giving rise to a cutoff wavelength such that below this, the modes are quasibound and cannot be excited anymore [38, 39] prohibiting the coupling of incident radiation with shorter wavelengths to SP's [38]. For the bare gold structure, the resonant behavior of the plasmons starts at 550 nm, while for the modified structures with only one layer of $MX_2$ the cutoff wavelength is at 650 nm, increasing with the number of layers of $MX_2$ as it can be seen

in Fig. 3. The FWHM for the modified structures broadens with the increase of number of the $MX_2$ layers. This broadening is caused by the rather high imaginary part of the $MX_2$ refractive indices. This also leads to a finite value of the reflectivity at resonance, which increases monotonically with the number of layers.

The minimum of reflectivity is increased with incidence radiation wavelength from 0.05% at 650 nm to almost 25% for 1400 nm. Reflectivity response at 1400 nm shows that the plasmon resonance arises approximately at the same resonance angle for all structures, and these findings are in agreement with the results obtained previously calculating the dispersion relations, where it was shown that the effective refractive indices of investigated structures become very close (Fig. 3). To clarify the differences for various $MX_2$ configurations, we examined the cross sections of the reflectivity map illustrated in Fig. 3 for three different wavelengths, i.e., 700, 900, and 1300 nm, respectively, and the corresponding plots are presented in Fig. 4. The associated phase response is shown in Fig. 5.

First of all, a significant difference between the bare structure and the modified structures can be seen at shorter wavelengths, in the proximity of the cutoff, in terms of both reflectivity and phase response. For the modified structures, the reflectivity curves indicate that the value of the resonant minimum, as well as the width of the resonant dip, increase monotonically with increasing number of additional $MX_2$ layers (Fig. 4). For example, at 700 nm, when 6 layers are added, the resonance angle shifts from 68.53° for the bare structure with more than 10° to the following values: 83.5° in the case of $MoS_2$. 82.68° for $WS_2$, and 81.04° for $WSe_2$, respectively.

With 6 layers of $MoSe_2$, the resonance angle's shift is considerable lower, reaching only the value of 76.55°. This behavior is determined by the high value of the imaginary part of the $MoSe_2$ refractive index in comparison with the other three
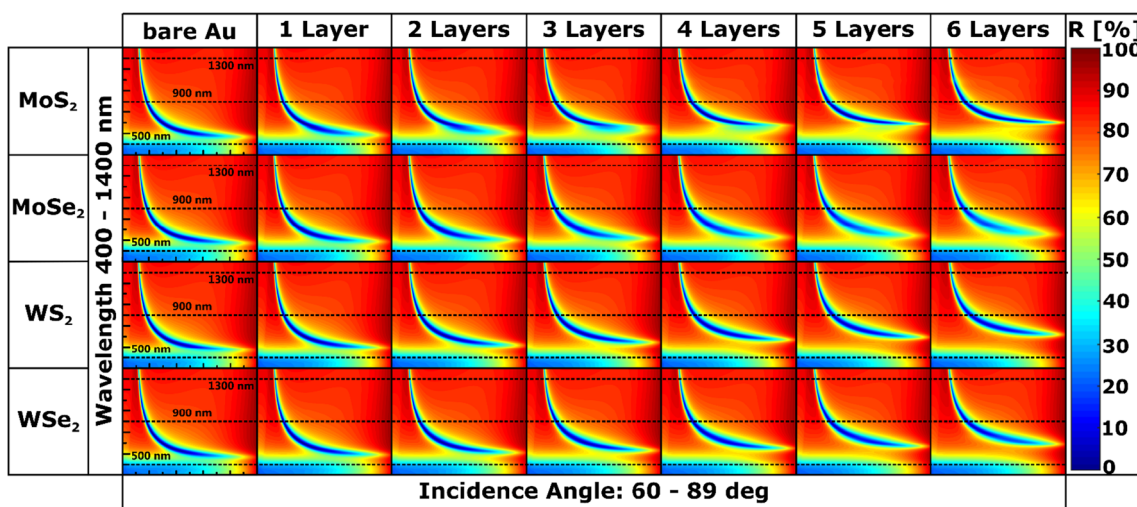


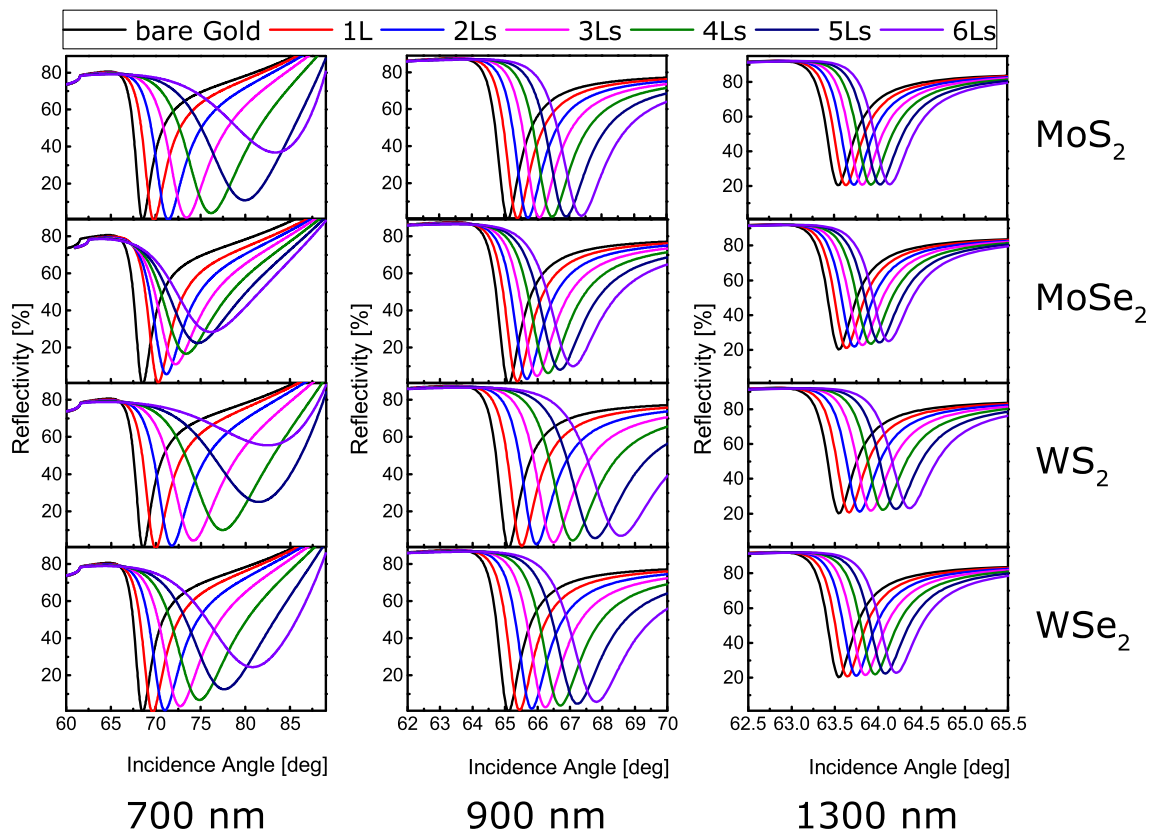Fig. 3 Sensors' dispersion curves for different numbers of $MX_2$ layers

**Fig. 4** Cross sections of the reflectivity maps at operating wavelengths of 600, 900, and 1300 nm, respectively
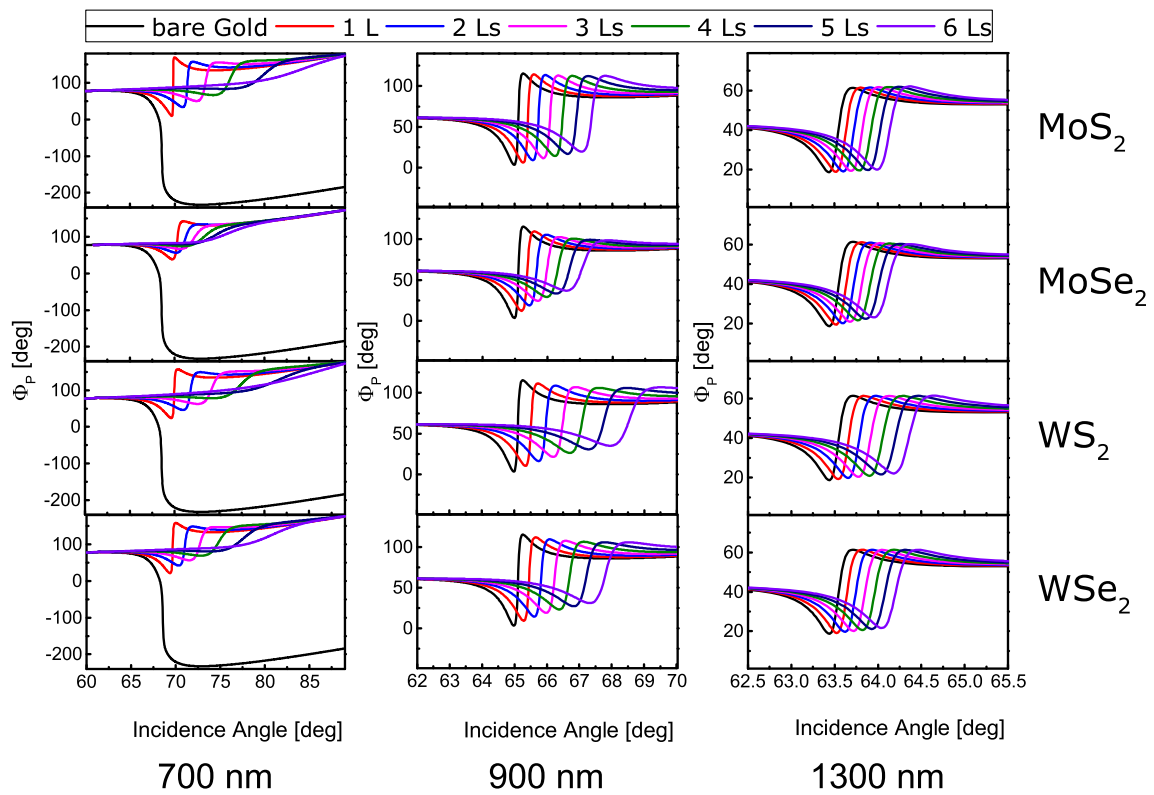


**Fig. 5** Phase response for TM polarized incident light at operating wavelengths of 600, 900, and 1300 nm, respectively

investigated dichalcogenides. In the same time, the corresponding reflectivity values increase significantly even for 2 additional layers, whereas at least 4 or 5 layers are necessary for the other types of $MX_2$ to get a comparable result. Furthermore, the dramatic increase of the reflectivity minima for the structures modified with 6 layers of disulfides should be mentioned, reaching 55% for $WS_2$. Analyzing the phase response at the same wavelength of 700 nm, it can be seen that it changes significantly when the bare structure is modified, getting a sharper aspect for the first 3 layers, while for the supplementary ones becoming shallower due to the increased minimum of the reflectivity. It is notable that the main change in phase is observed in the vicinity of resonance angle, where the intensity of the reflected radiation is almost zero. Consequently, despite the good reflectivity response of the structure with $MoSe_2$, it exhibits the lowest phase change of about 91°, whereas the unmodified structure reaches 303°. At 900 nm, the displacement of the resonance angle as a function of layer's number is small for all structures, including the bare one, and it is blue shifted with almost 4° in comparison with

the response obtained at 700 nm, as can be observed in Fig. 4. When the $MX_2$ layers were added, the resonance angle also suffers a red-shift, but it is considerable smaller, with a maximum of 3.5° for the $WS_2$-based configuration. In terms of the phase response, the structure also presents initially a sharp change (Fig. 5) and, after modification, a smaller red-shift, along with preserving the sharp change. Highest reflectivity of 9.88% was found for the structure with 6 layers of $MoSe_2$, the rest of the structures exhibiting reflectivities lower than 7%, the smallest one 2.31% was exhibited by 6 layers of $MoS_2$ while for the bare structure was 0.73% with 0.3% greater than the one obtained for the same structure at 700 nm. At longer wavelengths, the minimum of reflectivity is increased for all structures including the bare one, reaching 20% as can be seen in Fig. 4. Concurrently, adding the $MX_2$ layers, the resonance angles are blue shifted, even more than the ones at 900 nm, but the curves' shape is unaltered. The phase response trend is similar for all materials, but the sharp phase change is lost due to the higher minimum of the reflectivity (Fig. 5).
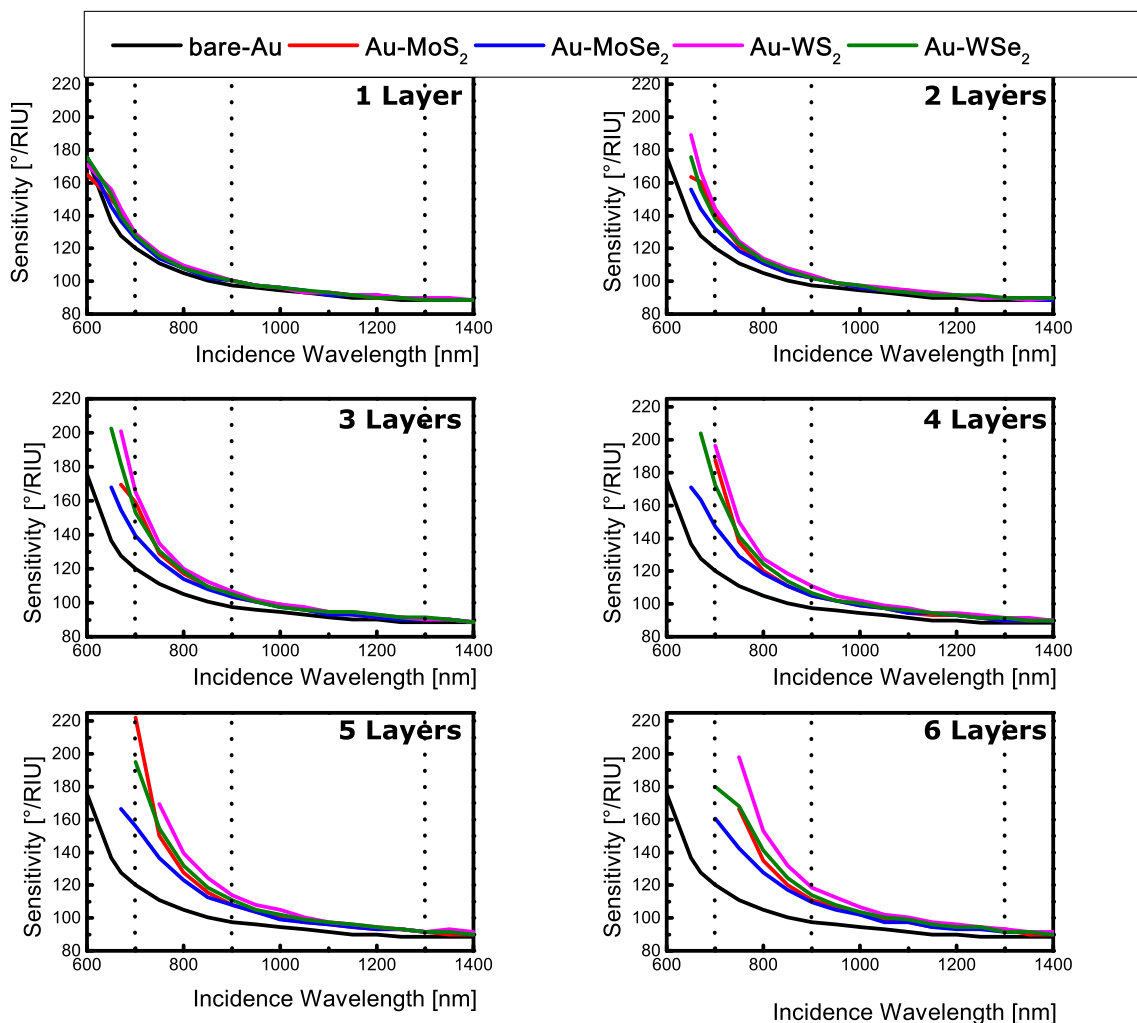


Fig. 6 Sensors' sensitivity in reflectivity for the entire range of wavelengths in VIS and NIR parts of the spectrum
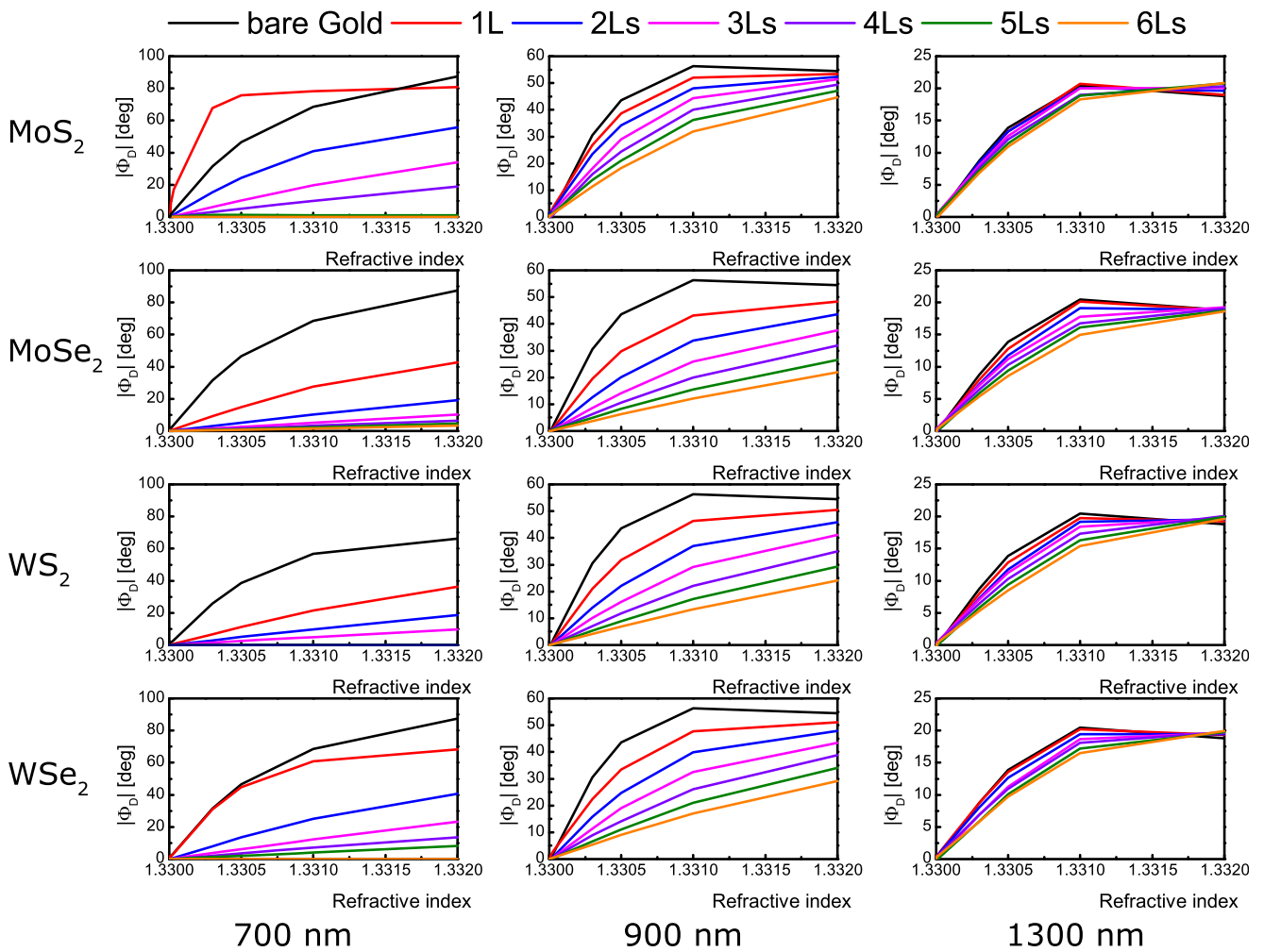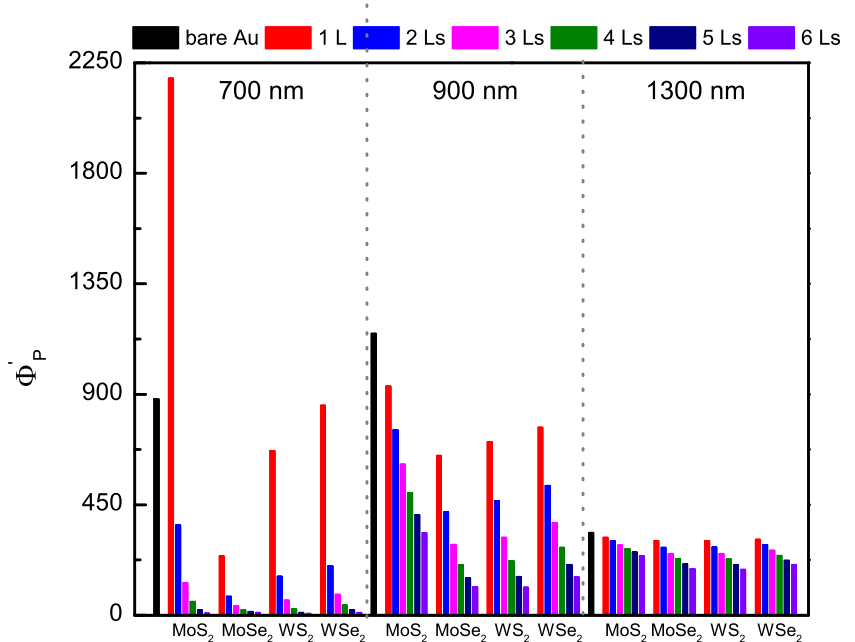
**Fig. 7** Variation of differential phase with the sensing medium's refractive index at operating wavelengths of 600, 900, and 1300 nm, respectively

**Fig. 8** First derivative of phase for the TM polarized incident light for all proposed structures at operating wavelengths of 600, 900, and 1300 nm, respectively

Next, we investigated the variation of wavelength sensitivity with change in refractive index of analyte, as small as 0.002 RIU, analyzing both the reflectivity and phase response. The reflectivity sensitivity was calculated using the formula (10) and the resulted data were plotted for different wavelengths in Fig. 6. It can be observed firstly that the modified structures present an enhanced sensitivity comparing with the bare one, observable even when a single monolayer is added. In this case, a small improvement can be observed, with a maximum difference between sensitivities of about 10 deg/RIU for Au-WS$_2$ and Au-MoS$_2$ at 650 nm. Progressively, when more layers are added, this difference increases, showing a significant enhancement in sensitivity, but it should be noted that the resonance arises at longer wavelengths, beyond 700 nm for 6 layers. The highest sensitivity achieved was 220 deg/RIU at 700 nm for the structure containing 5 layers of MoS$_2$, corresponding to an increase of sensitivity with 63% in comparison to the bare structure. Regarding the rest of interrogated wavelength range, the sensitivity enhancement slightly decrease with increase of the wavelength, WS$_2$ leading to the best performances, with 118 deg/RIU at 900 nm that represents an approx. 20% improvement. For longer wavelengths (> 1100 nm), all structures exhibit roughly the same sensitivity, with a minor improvement of sensing performances after modification, confirming the dispersion relations results (Fig. 2).

In order to explore the phase sensitivity at very small variations of the sensitive medium's refractive index, we analyzed the phase difference for all structures as a function of the sensing medium's refractive index when it is ranging from 1.33 to only 1.332. The differential phase variation as function of the change in sensitive medium's refractive medium, used subsequently to calculate the phase sensitivity employing the Eq. (11) for the three reference wavelengths, 700, 900, and 1300 nm, respectively, is shown in Fig. 7. The highest sensitivity is $9 \times 10^5$ deg/RIU for a change $\Delta n = 10^{-6}$ is obtained for the structure modified with one layer of MoS$_2$ at 700 nm, fivefold higher than the bare gold structure at the same wavelength. On the contrary, MoSe$_2$, WS$_2$, and WSe$_2$ do not enhance the phase sensitivity, and if Au-WSe$_2$ sensitivity is only 5% lower, the other two types lead to approximately only half of the bare structure potential. For wavelengths longer than 1000 nm, the phase difference decrease even more, but the differences between the bare and the MX$_2$ modified structures are smaller indicating an approximatively similar sensitivity in phase, as it was expected from SP's dispersion relations (Fig. 3) and reflectivity maps (Fig. 4), respectively.

It should be mentioned that MoS$_2$-based modification of the SPR structures exhibits at all wavelengths the best performances in terms of phase response in comparison with the rest of MX$_2$ types analyzed. Also, in comparison with the

sensitivity in reflectivity, the phase sensitivity decreases with the increase of refractive index changes, but due to the excessive energy loss in the additional MX$_2$ layers the phase decrease with the increase of the number of layers added [40]. Even though the phase sensitivity is reduced for a change in refractive index of $2 \times 10^{-3}$ RIU for all structures, the phase response was higher than the reflectivity response achieving sensitivities greater than the ones in reflectivity; however, the main drawback of phase response is represented by the complex experimental setup [41–44]. To further clarify the sensors performances in phase, we have represented in Fig. 8 the first derivative of phase response for a sensing medium's refractive index of 1.33, in order to find the sharpest phase change for the investigated structures. It can be easily seen that the phase sensitivity of the bare structure increases from $1.13 \times 10^5$ at 700 nm to $1.21 \times 10^5$ deg/RIU at 900 nm, the enhancement being attributed to the sharper phase response, as can be seen in Fig. 7. On the contrary, the structure containing one layer of MoS$_2$ reaches the highest change at 700 nm, and starts to decrease at longer wavelengths. At 1300 nm, the bare structure presents a significant diminish of the phase change that become comparable with the ones obtained for the modified ones.

## Conclusions

A SPR-based sensor with different numbers of TMDC monolayers added to a standard Kretschmann configuration was systematically investigated exploring the space of geometrical and material parameters in terms of the dispersion relations, reflectivity maps, and both reflectivity and phase sensitivities, respectively. The sensors' response was correlated with the properties of SPs at the interface between both gold-sensing medium and gold-MX$_2$-sensing medium, found by analyzing the dispersion relations. The results indicate that coating the gold layer with MX$_2$ monolayers, the sensors' sensitivity is improved, but as was revealed by the dispersion relations, the improvement was significantly enhanced for smaller wavelengths (< 1100 nm) both in phase and reflectivity. The phase response is more sensitive than the one in reflectivity for the entire range of the refractive indices considered for the sensing medium. It was shown that varying the number of MX$_2$ and the wavelength we can tune the sensors performance properly for the desired applications. For example, to monitor the hybridization reactions of ssDNA, when the immobilized DNA molecules considerably increase the refractive index of the sensing medium near the gold layer, the reflectivity response is preferable, whereas for gas or temperature sensing, where the variations of refractive index are very small, the phase response should be appropriate.

# References

1. Cada M, Blazek D, Pistora J, Postava K, Siroky P (2015) Theoretical and experimental study of plasmonic effects in heavily doped gallium arsenide and indium phosphide. Opt Mater Express 5:2

2. Xiangjun L, Jian S, John XJZ (2015) Integrated terahertz surface plasmon resonance on polyvinylidene fluoride layer for the profiling of fluid reflectance spectra. Plasmonics 11(4):1093–1100

3. Economou EN (1969) Surface plasmons in thin films. Phys Rev 182:2

4. Kretschmann E, Raether H (1968) Radiative decay of non radiative surface plasmons excited by light. Z Naturforsch A 23:2135–2136

5. Heinz R (1988) Surface Plasmons on Smooth and Rough Surfaces and on Gratings. Springer-Verlag, Berlin Heidelberg

6. Wei L, Rujing W, Hairong L, Jieting K, Xinhua Z, He H, Xiaobo H, Wei H (2019) Simultaneous measurement of refractive index and temperature for prism-based surface plasmon resonance sensors. Opt Express 27(2):2019

7. Chlebus R, Chylek J, Ciprian D, Hlubina P (2018) Surface plasmon resonance based measurement of the dielectric function of a thin metal film. Sensors 18:3693

8. Breveglieri G, Gallo TE, Travan A, Pellegatti P, Guerra G, Gambari R, Borgatti M (2016) Surface plasmon resonance analysis to detect the $\beta^+$ IVSI-110 thalassemia mutation in circulating cell-free fetal DNA. Clin Chim Acta 462:133–134

9. Breveglieri G, Bassi E, Carlassara S, Cosenza LC, Pellegatti P, Guerra G, Finotti A, Gambari R, Borgatti M (2016) Y-chromosome identification in circulating cell-free fetal DNA using surface plasmon resonance. Prenat Diagn 36:353–361

10. Majka J, Speck C (2007) Analysis of protein-DNA interactions using surface plasmon resonance. Adv Biochem Engin/Biotechnol 104:13–36

11. Rajan J, Anuj KS (2010) Design of a silicon-based plasmonic biosensor chip for human blood-group identification. Sensors Actuators B Chem 145:200–204

12. Jijo L, Vignesh S, Mamatha B, Santhosh C, Rajeev KS (2018) Real-time and rapid detection of *Salmonella typhimurium* using an inexpensive lab-built surface plasmon resonance setup. Laser Phys Lett 15:075701

13. Kabashin AV, Evans P, Pastkovsky S, Hendren W, Wirtz GA, Atkinson R, Pollard R, Podolskiy VA, Zayats AV (2009) Plasmonic nanorod metamaterials for biosensing. Nat Mater 8:867–871

14. Rob PHK (2008) Physics of surface plasmon resonance. In: Richard BMS, Anna JT (eds) Handbook of surface plasmon resonance. The Royal Society of Chemistry, UK, pp 15–34

15. Stepan AZ, Anton VS, Elena RS, Vladimir MM, Shirshov YM (2002) Bimetallic layers increase sensitivity of affinity sensors based on surface plasmon resonance. Sensors 2:62–70

16. Sarah F, Naseer S, Zul AZJ, Prabakaran P (2017) Surface plasmon resonance sensor sensitivity enhancement using gold-dielectric material. Int J Nanoelectr Mater 10:149–158

17. Lahav A, Atef S, Ibrahim A (2009) Surface plasmon sensor with enhanced sensitivity using top nano dielectric layer. J Nanophotonics 3(1):031501

18. Yufeng Y, Xiantong Y, Qinlinq O, Yonghong S, Jun S, Junle Q, Ken-Tye Y (2018) Highly anisotropic black phosphorus-graphene hybrid architecture for ultrasensitive plasmonic biosensing: theoretical insight. 2D Materials 5:025015

19. Sherif HEG, Munsik C, Young LK, Kyung MB (2016) Dispersion curve engineering of $TiO_2$/silver hybrid substrates for enhanced surface plasmon resonance detection. Sensors 16:1442

20. Molitor F, Guttinger J, Stampfer C, Droscher S, Jacobsen A, Ihn T, Ensslin K (2011) Electronic properties of graphene nanostructures. J Phys Condens Matter 23(24):243201

21. Li D, Wensi Z, Xiaoqing Y, Zhenping W, Zhiqiang S, Gang W (2016) When biomolecules meet graphene: from molecular level interactions to material design and applications. Nanoscale 8(47):19491–19509

22. Leiming W, Chu HS, Koh WS, Li EP (2010) Highly sensitive graphene biosensors based on surface plasmon resonance. Opt Express 18(14):14395–14400

23. Leiming W, Jun G, Xiaoyu D, Xiang XJ, Dianyuan F (2017) Sensitivity enhanced by $MoS_2$-graphene hybrid structure in guided-wave surface plasmon resonance biosensor. Plasmonics 13:281–285

24. Jinguang T, Li J, Huifang C, Yiqin W, Ken-Tye Y, Erik F, Sailing H (2018) Graphene-bimetal plasmonic platform for ultra-sensitive biosensing. Opt Commun 410:817–823

25. Szunerits S, Maalouli N, Wijaya E, Vilcot JP, Boukherroub R (2013) Recent advances in the development of graphene-based surface plasmon resonance (SPR) interfaces. Anal Bioanal Chem 405(5):1435–1443

26. Chang Lu YL, Yibin Y, Juewen L (2017) Comparison of $MoS_2$, $WS_2$ and graphene oxide for DNA adsorption and sensing. Langmuir 33(2):630–637

27. Saifur R, Rabiul H, Ritka KA, Shamim A (2018) A novel graphene coated surface plasmon resonance biosensor with tungsten disulfide ($WS_2$) for sensing DNA hybridization. Opt Mater 75:567–573

28. Minghong W, Yanyan H, Shouzhen J, Chao Z, Cheng Y, Tingyin N, Xioyun L, Chonghui L, Wenyuan Z, Baoyuan M (2017) Theoretical design of a surface plasmon resonance sensor with high sensitivity and high resolution based on graphene-$WS_2$ hybrid nanostructures and Au-Ag bimetalic film. RSC Adv 7:47177–47182. https://doi.org/10.1039/C7RA08380G

29. Qinling O, Shuwen Z, Li J, Liying H, Gaixia X, Xuan-Quyen D, Jun Q, Sailing H, Junle Q, Philippe C, Ken-Tye Y (2016) Sensitivity enhancement of transition metal dichalcogenides/silicon nanostructured surface plasmon resonance biosensor. Sci Rep 6:28190

30. Saifur R, Shamim A, Rabiul H, Biplob H, Ismail H (2017) Design and numerical analysis of highly sensitive Au-$MoS_2$–graphene based hybrid surface plasmon resonance biosensor. Opt Commun 396(1):36–43

31. Qingling O, Shuwen Z, Xuan-Quyen D, Philippe C, Ken-Tye Y (2016) Sensitivity enhancement of $MoS_2$ nanosheet based surface plasmon resonance biosensor. Procedia Engineering 140:134–139. https://doi.org/10.1016/j.proeng.2015.08.1114

32. Saifur R, Shaikh SN, Shamim A, Lway FA, Maksudur R, Ritka KA (2019) Design and numerical analysis of a graphene-coated fiber-optic SPR biosensor using tungsten disulfide. Photonics Nanostruct Fundam Appl 33:29–35

33. Sexton BA, Feltis BN, Davis TJ (2008) Characterisation of gold surface plasmon resonance sensor substrates. Sensors Actuators A 141:471–475

34. Hyuk RG, Seong HL (2010) Spectral and angular responses of surface plasmon resonance based on the Kretschmann prism configuration. Mater Trans 51(6):1150–1155

35. Hsiang-Lin L, Chih-Chiang S, Shen-Han S, Chang-Lung H, Ming-Yang L, Jong L (2014) Optical properties of monolayer transition metal dichalcogenides probed by spectroscopic ellipsometry. Appl Phys Lett 105:20

36. Pradeep KM, Rajan J (2012) Chalcogenide prism and graphene multilayer based surface plasmon resonance affinity biosensor for high performance. Sensors Actuators B Chem 169:161–166

37. William LB (2006) Surface plasmon-polariton length scales: a route to sub wavelength optics. J Opt A Pure Appl Opt 8:S87–S93

38. Stefan Alexander M (2007) Plasmonics: fundamentals and applications. Springer US, New York

39. Dionne JA, Sweatlock LA, Atwater HA, Polman A (2005) Planar metal plasmon waveguides: frequency-dependent dispersion, propagation, localization, and loss beyond the free electron model. Phys Rev B 72:075405

40. Hu WQ, Liang EJ, Ding P, Cai GW, Xue QZ (2009) Surface plasmon resonance and field enhancement in #-shaped gold wires metamaterial. Opt Express 17:21843–21849

41. Hai-Pang C, Jing-Lun L, Railing C, Sheng-Yu S, Pui Tak L (2005) High-resolution angular measurement using surface plasmon-resonance via phase interrogation at optimal incident wavelengths. Opt Lett 30:20

42. Petr H, Dalibor C (2017) Spectral phase shift if surface plasmon resonance in the Kretschmann configuration: theory and experiment. Plasmonics 12(4):1071–1078

43. Chie-Ming W, Zhi-Cheng J, Shen-Fen J, Liann-Be C (2003) High-sensitivity sensor based on surface plasmon resonance and heterodyne interferometry. Sensors Actuators B 92:133–136

44. Wei G, Shouzhen J, Zhen L, Chonghui L, Jihua X, Jie P, Yanyan H, Baoyuan M, Aihua L, Chao Z (2019) Experimental and theoretical investigation for surface plasmon resonance biosensor based on graphene/Au film/D-POF. Opt Express 27(3):3483–3495

**Publisher's Note** Springer Nature remains neutral with regard to jurisdictional claims in published maps and institutional affiliations.